A Landing Approach Guidance Scheme for Unpowered Lifting Vehicles

WILLIAM C. HOFFMAN* AND JOHN ZVARA†
Aerospace Systems Inc., Lexington, Mass.

AND

ARTHUR E. BRYSON JR.‡
Stanford University, Stanford, Calif.

The subsonic glide of a lifting vehicle is approximated by treating heading angle and the two position coordinates in the horizontal plane as state variables, altitude as independent variable, and angle of attack and bank angle as control variables. By considering perturbations about a nominal trajectory and minimizing a performance index which is quadratic in both the terminal state variable errors and the enroute control variable deviations, a simple linear guidance law is obtained, whose feedback gains are functions of altitude. During flight the actual heading and position are estimated from measurements and their deviations from nominal are used to calculate optimal corrections to the nominal control histories. Simulation results obtained using the complete point-mass vehicle dynamics indicate the scheme can successfully handle a variety of off-nominal conditions.

Nomenclature

g = gravitational force per unit mass = 9.80 m/sec²
h = altitude = $-z$,m
l = characteristic length of vehicle = $2m\eta/\rho C_{L\alpha}S$, m
m = mass of vehicle, kg
q = dynamic pressure = $\rho V^2/2$, N/m^2
$\mathbf{u}$ = control vector of linearized, simplified system; defined in Eq. (26)
$w_{x,y}$ = x and y components of wind, respectively, m/sec
x,y,z = position coordinates, m
$\mathbf{x}$ = state vector of linearized, simplified system; defined in Eq. (26)
$\mathbf{B}$ = penalty matrix on enroute control deviations; defined in Eq. (30)
$\mathbf{C}$ = matrix of guidance feedback gains; defined in Eq. (32)
C_{D_0} = aerodynamic drag coefficient for zero lift
$C_{L\alpha}$ = aerodynamic lift curve slope = $(\partial L/\partial\alpha)/qS$, deg^{-1}
$C_{\alpha x}$ = feedback gain for α due to error in x, deg/m
$C_{\alpha y}$ = feedback gain for α due to error in y, deg/m
$C_{\alpha\psi}$ = feedback gain for α due to error in ψ, deg/deg
$C_{\phi x}$ = feedback gain for ϕ due to error in x, deg/m
$C_{\phi y}$ = feedback gain for ϕ due to error in y, deg/m
$C_{\phi\psi}$ = feedback gain for ϕ due to error in ψ, deg/deg
D = aerodynamic drag force, N
$\mathbf{F}$ = homogeneous matrix of linearized, simplified system; defined in Eq. (27)
$\mathbf{G}$ = forcing matrix of linearized, simplified system; defined in Eq. (28)
J = performance index; defined in Eq. (29)
L = aerodynamic lift force, N
R = local radius of helix for quasi-steady glide = $V^2(\cos\gamma)/g\tan\phi$, m
S = aerodynamic reference area of vehicle, m²
$\mathbf{S}$ = Riccati matrix; defined by Eqs. (33) and (34)
$\mathbf{S}_f$ = penalty matrix on terminal state variable deviations, defined in Eq. (30)
V = velocity of vehicle, m/sec
α = angle of attack, deg
α_0 = angle of attack for zero lift, deg
$\bar{\alpha}$ = modified angle of attack = $\eta(\alpha - \alpha_0)$
γ = flight path angle, deg
δ = minimum drag/lift ratio of vehicle = $2(\eta C_{D_0}/C_{L\alpha})^{1/2}$
$\delta(\ )$ = perturbation from nominal of quantity indicated = $(\ ) - (\ )_N$
δx_f = weighting parameter on terminal downrange error, m
δy_f = weighting parameter on terminal crossrange error, m
$\delta\psi_f$ = weighting parameter on terminal heading error, deg
$\delta\alpha_m$ = weighting parameter on enroute α perturbations, deg
$\delta\phi_m$ = weighting parameter on enroute ϕ perturbations, deg
η = aerodynamic efficiency factor ($0 \leq \eta \leq 1$)
ρ = atmospheric density, kg/m³
ϕ = bank angle, deg
ψ = heading angle, deg

Subscripts

f = final value
m = maximum allowable or desirable value
0 = initial value or zero-lift value
N = nominal value

Introduction

A PICTORIAL description of the terminal region of flight of a lifting vehicle is shown in Fig. 1. The figure illustrates the two types of landing approach patterns that may be used by unpowered lifting vehicles: a minimum-turn approach and a spiral approach. As the name implies, a minimum-turn approach is one which uses the smallest heading change necessary to line up with the landing direction; such a turn is always less than or equal to 180°. A spiral approach is one which involves a turn of more than 180°.

A number of guidance concepts for lifting entry vehicles have appeared in the technical literature (cf., Refs. 1–5). Most of these systems are concerned with the initial phase of entry and are generally capable of delivering the vehicle to the vicinity of the landing site with position errors of a few kilometers (km), and with velocity errors on the order of 10 meters per second (m/sec). This paper presents a simple but highly accurate landing approach guidance scheme for a lifting entry vehicle.[6] A precise terminal guidance system such as this one will be vital to these advanced vehicles which require the capability to perform routine or emergency landings at night or under marginal weather conditions.

Presented as Paper 69-865 at the AIAA Guidance Control and Flight Mechanics Conference, Princeton, N.J., August 18–20, 1969; submitted August 25, 1969; revision received October 23, 1969. Work supported in part by NASA/ERC Contract NAS 12-99.

* Project Engineer; formerly with Kaman AviDyne, Burlington, Mass. Member AIAA.

† President; formerly with Kaman AviDyne, Burlington, Mass. Associate Fellow AIAA.

‡ Chairman, Department of Applied Mechanics.

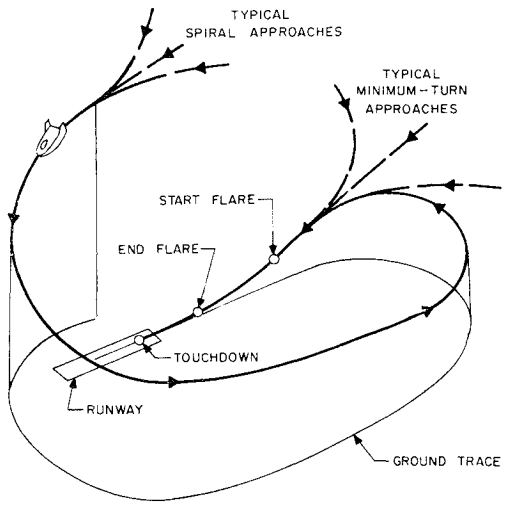

Fig. 1 Typical landing approaches.

Equations of Motion and Simplified Model

A lifting body vehicle may be represented as a point mass acted upon by aerodynamic and gravitational forces. The coordinate system and nomenclature used in the analysis are illustrated in Fig. 2. The origin of the coordinate system is at the runway touchdown point; the x axis is in the horizontal plane, parallel to the runway and positive in the landing direction; the z axis is positive down along the local vertical; and the y axis forms a right-hand orthogonal system. The flight path angle γ is positive below the local horizontal and the bank angle ϕ denotes a rotation of the lift vector about the velocity vector away from the vertical plane.

The equations of motion may be written as

$$m\dot{V} = -D + mg\sin\gamma \tag{1}$$

$$mV\dot{\gamma} = -L\cos\phi + mg\cos\gamma \tag{2}$$

$$mV\cos\gamma\,\dot{\psi} = L\sin\phi \tag{3}$$

$$\dot{x} = V\cos\gamma\cos\psi \tag{4}$$

$$\dot{y} = V\cos\gamma\sin\psi \tag{5}$$

$$\dot{z} = V\sin\gamma \tag{6}$$

The six state variables of the system are the velocity V, the flight path angle γ, the heading angle ψ and the position coordinates x, y, z; the angle of attack α and the bank angle ϕ are the control variables; and the aerodynamic lift L and drag D are functions of α, V and z.

Quasi-Steady Approximation

Typical lifting body entry vehicles have been found to approach a quasi-steady subsonic glide for a wide range of initial conditions. That is, $\dot{V}$ and $\dot{\gamma}$ become negligible. Thus, Eqs. (1–3) may be approximated as

$$D = mg\sin\gamma \tag{7}$$

$$L = mg\cos\gamma\sec\phi \tag{8}$$

$$\dot{\psi} = g(\tan\phi)/V \tag{9}$$

For constant α and ϕ, Eqs. (4–9) approximate the flight path as a descending helix with slowly changing helix angle γ and radius R as shown in Fig. 3. The quasi-steady flight path angle and velocity are implicitly determined as functions of α and ϕ by Eqs. (7) and (8), and the radius of turn is given by

$$R = V(\cos\gamma)/\dot{\psi} = V^2(\cos\gamma)/g\tan\phi \tag{10}$$

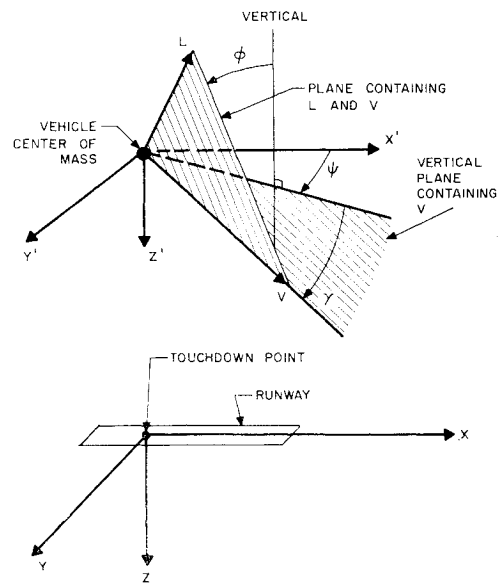

Fig. 2 Coordinate system and nomenclature.

Altitude as Independent Variable

If the altitude, $h = -z$, is used instead of time as the independent variable, the motion of the glider may be expressed in terms of only three state variables. By dividing Eq. (6) into Eqs. (4, 5, and 9), and using Eq. (10), we obtain the following simplified equations:

$$dx/dh = -\mathrm{ctn}\gamma\cos\psi \tag{11}$$

$$dy/dh = -\mathrm{ctn}\gamma\sin\psi \tag{12}$$

$$d\psi/dh = -(\mathrm{ctn}\gamma)/R \tag{13}$$

The state variables of the reduced system are x, y and ψ; the independent variable is h; and the control variables are α and ϕ. The parameters V, γ and R are given implicitly by Eqs. (7, 8, and 10).

Aerodynamic Approximation

The aerodynamic forces may be closely approximated by assuming lift to be linear and drag to be quadratic in α; i.e.,

$$L = qS\,C_{L\alpha}(\alpha - \alpha_0) \tag{14}$$

$$D = qS[C_{D_0} + \eta C_{L\alpha}{}^2(\alpha - \alpha_0)^2] \tag{15}$$

where q is the dynamic pressure, S is the aerodynamic reference area, $C_{L\alpha}$ is the lift coefficient slope, α_0 is the angle of attack for zero lift, C_{D_0} is the zero-lift drag coefficient, and η is an efficiency factor ($0 \leq \eta \leq 1$). In general, $C_{L\alpha}$, α_0, C_{D_0} and η are functions of Mach number, but for subsonic flight they are very nearly constant.

Equations (14) and (15) may be used to rewrite Eqs. (7, 8, and 10) as

$$V^2/gl = (\cos\gamma)/\bar{\alpha}\cos\phi \tag{16}$$

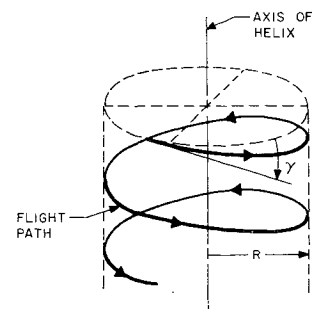

Fig. 3 Flight path as a locally descending helix.

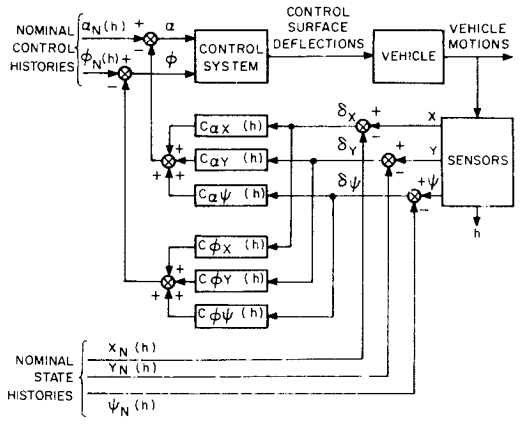

Fig. 4 Implementation of the guidance scheme.

$$\tan\gamma = (\bar{\alpha} + \delta^2/4\bar{\alpha})\sec\phi \tag{17}$$

$$R = l(\cos^2\gamma)/\bar{\alpha}\sin\phi \tag{18}$$

where $l = 2m\eta/\rho C_{L\alpha}S$ is a characteristic length of the vehicle, $\delta = (2\eta C_{D_0}/C_{L\alpha})^{1/2}$ is its minimum drag/lift ratio; and $\bar{\alpha} = \eta(\alpha - \alpha_0)$ is the modified angle of attack. Equations (16–18) determine the quasi-steady velocity V, flight path angle γ and radius of turn R in terms of the altitude h and the control variables α and ϕ.

The simplified system is completely specified by Eqs. (11–13, 17, and 18). At any given altitude, the control variables α and ϕ determine R and γ through Eqs. (17) and (18).§ These, together with the current values of the state variables (x,y,ψ), completely determine the rates of change of (x,y,ψ) with altitude.

Linearized Equations

The equations of motion of the simplified model may be linearized by taking first-order perturbations about a nominal trajectory. Using vector-matrix notation, the perturbation form of Eqs. (11–13) may be written as

$$\frac{d}{dh}\begin{bmatrix}\delta x\\ \delta y\\ \delta\psi\end{bmatrix} = \begin{bmatrix}0 & 0 & \operatorname{ctn}\gamma\sin\psi\\ 0 & 0 & -\operatorname{ctn}\gamma\cos\psi\\ 0 & 0 & 0\end{bmatrix}_N\begin{bmatrix}\delta x\\ \delta y\\ \delta\psi\end{bmatrix} + \begin{bmatrix}\cos\psi\csc^2\gamma & 0\\ \sin\psi\csc^2\gamma & 0\\ (\csc^2\gamma)/R & (\operatorname{ctn}\gamma)/R^2\end{bmatrix}_N\begin{bmatrix}\delta\gamma\\ \delta R\end{bmatrix} \tag{19}$$

where the subscript N indicates the quantity is evaluated along the nominal trajectory, and the perturbation quantities are defined by $\delta(\ ) = (\ ) - (\ )_N$.

Similarly, the perturbation versions of Eqs. (17) and (18) are

$$\begin{bmatrix}\delta\gamma\\ \delta R\end{bmatrix} = \begin{bmatrix}\partial\gamma/\partial\alpha & \partial\gamma/\partial\phi\\ \partial R/\partial\alpha & \partial R/\partial\phi\end{bmatrix}_N\begin{bmatrix}\delta\alpha\\ \delta\phi\end{bmatrix} \tag{20}$$

where the elements of the matrix are

$$\partial\gamma/\partial\alpha = \eta[1 - \delta^2/4\bar{\alpha}^2]\cos^2\gamma\sec\phi \tag{21}$$

$$\partial\gamma/\partial\phi = (\sin 2\gamma\tan\phi)/2 \tag{22}$$

$$\frac{\partial R}{\partial\alpha} = -\eta R\left[\frac{1}{\bar{a}} + \frac{\sin 2\gamma}{\cos\phi}\left(1 - \frac{\delta^2}{4\bar{\alpha}^2}\right)\right] \tag{23}$$

$$\partial R/\partial\phi = -R[\operatorname{ctn}\phi + 2\tan\phi\sin^2\gamma] \tag{24}$$

and $\delta\alpha = \alpha - \alpha_N$; $\delta\phi = \phi - \phi_N$.

§ There are actually two values of α and ϕ which satisfy Eqs. (17) and (18) for each γ and R. The solution for the lower value of α, which corresponds to the "low" side of the L/D curve, was selected.

The substitution of Eq. (20) into Eq. (19) leads to the desired set of linear perturbation equations

$$\mathbf{dx}/dh = \mathbf{Fx} + \mathbf{Gu} \tag{25}$$

where the state vector $\mathbf{x}$ and the control vector $\mathbf{u}$ are defined as

$$\mathbf{x} = \begin{bmatrix}\delta x\\ \delta y\\ \delta\psi\end{bmatrix}, \qquad \mathbf{u} = \begin{bmatrix}\delta\alpha\\ \delta\phi\end{bmatrix} \tag{26}$$

and the matrices $\mathbf{F}$ and $\mathbf{G}$ are given by

$$\mathbf{F} = \begin{bmatrix}0 & 0 & \operatorname{ctn}\gamma\sin\psi\\ 0 & 0 & -\operatorname{ctn}\gamma\cos\psi\\ 0 & 0 & 0\end{bmatrix}_N \tag{27}$$

$$\mathbf{G} = \begin{bmatrix}\cos\psi\csc^2\gamma & 0\\ \sin\psi\csc^2\gamma & 0\\ (\csc^2\gamma)/R & (\operatorname{ctn}\gamma)/R^2\end{bmatrix}_N\begin{bmatrix}\partial\gamma/\partial\alpha & \partial\gamma/\partial\phi\\ \partial R/\partial\alpha & \partial R/\partial\phi\end{bmatrix}_N \tag{28}$$

Quadratic Synthesis Technique

Having described the approximate motion of the vehicle in the vicinity of the nominal trajectory, we may now apply the quadratic synthesis technique[7] to find a linear feedback guidance law. A convenient performance index to choose for this purpose is one which is a quadratic function of the enroute control perturbations and the terminal state variable errors; i.e.,

$$J = \frac{1}{2}(\mathbf{x}^T\mathbf{S}_f\mathbf{x})_{h=h_f} + \frac{1}{2}\int_{h_0}^{h_f}(\mathbf{u}^T\mathbf{B}\mathbf{u})dh \tag{29}$$

where h_0 and h_f are, respectively, the initial and final altitudes.¶ The matrices $\mathbf{S}_f$ and $\mathbf{B}$ weight the penalties associated with the terminal state variable errors and the use of

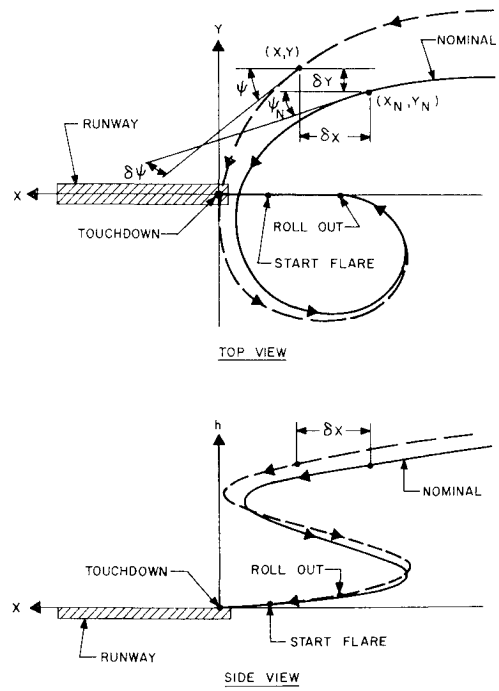

Fig. 5 Typical performance of the guidance scheme.

¶ If it were desirable to maintain the vehicle close to the nominal path (e.g. for air traffic control), a quadratic penalty term on enroute state variable deviations could be included in the integrand of Eq. (29).

Table 1 Vehicle parameters and performance weighting functions

Vehicle parameters			Weighting functions	
m	2721.5	kg	δx_f	100.0 m
S	12.91	m^2	δy_f	50.0 m
C_{L_α}	0.0223	deg^{-1}	$\delta \psi_f$	1.0 deg
α_0	−9.48	deg	$\delta \alpha_m$	3.0 deg
C_{D_0}	0.05946	—	$\delta \phi_m$	30.0 deg
η	0.3148			
δ	0.2737	—		

control deviations during the descent

$$\mathbf{S}_f = \begin{bmatrix} \delta x_f^{-2} & 0 & 0 \\ 0 & \delta y_f^{-2} & 0 \\ 0 & 0 & \delta \psi_f^{-2} \end{bmatrix}$$
$$\mathbf{B} = \frac{1}{h_f - h_0} \begin{bmatrix} \delta \alpha_m^{-2} & 0 \\ 0 & \delta \phi_m^{-2} \end{bmatrix} \quad (30)$$

The parameters δx_f, δy_f, $\delta \psi_f$, $\delta \alpha_m$ and $\delta \phi_m$ must be chosen to provide satisfactory terminal accuracy within limitations of allowable $\delta \alpha$ and $\delta \phi$. Usually, good estimates are the maximum acceptable values.

The minimization of the performance criterion, Eq. (29), subject to the perturbation equations of motion, Eq. (25), yields the linear feedback guidance law

$$\mathbf{u} = -\mathbf{C}(h)\mathbf{x} \quad (31)$$

where the feedback gain matrix $\mathbf{C}(h)$ is defined by

$$\mathbf{C} = \mathbf{B}^{-1}\mathbf{G}^T\mathbf{S} \quad (32)$$

and $\mathbf{B}^{-1}$ is the inverse of $\mathbf{B}$ [Eq. (30)], $\mathbf{G}^T$ is the transpose of $\mathbf{G}$ [Eq. (28)] and $\mathbf{S}$ is the solution of the matrix Ricatti equation

$$d\mathbf{S}/dh = -\mathbf{SF} - \mathbf{F}^T\mathbf{S} + \mathbf{SGB}^{-1}\mathbf{G}^T\mathbf{S} \quad (33)$$

with the boundary condition

$$\mathbf{S}(h_f) = \mathbf{S}_f \quad (34)$$

Guidance Scheme

The terminal guidance law is given by Eq. (31), which in expanded form is

$$\begin{bmatrix} \alpha \\ \phi \end{bmatrix} = \begin{bmatrix} \alpha_N(h) \\ \phi_N(h) \end{bmatrix} - \begin{bmatrix} C_{\alpha x}(h) & C_{\alpha y}(h) & C_{\alpha \psi}(h) \\ C_{\phi x}(h) & C_{\phi y}(h) & C_{\phi \psi}(h) \end{bmatrix} \times \begin{bmatrix} x - x_N(h) \\ y - y_N(h) \\ \psi - \psi_N(h) \end{bmatrix} \quad (35)$$

The implementation of the guidance scheme is summarized in Fig. 4. A nominal trajectory is selected and the corresponding feedback gains are calculated by means of Eqs. (32–34). The nominal state histories $[x_N(h), y_N(h), \psi_N(h)]$, the nominal control histories $[\alpha_N(h), \phi_N(h)]$, and the feedback gains $[C_{\alpha x}(h), C_{\alpha y}(h), C_{\alpha \psi}(h), C_{\phi x}(h), C_{\phi y}(h), C_{\phi \psi}(h)]$ are stored as functions of altitude in the airborne computer. During the landing approach, the state variables (and the altitude) are estimated from measurements and compared with the nominal values for that altitude. The deviations are then used to modify the stored nominal control histories by means of Eq. (35).

Figure 5 shows the horizontal and vertical projections of a typical nominal trajectory (solid) and a possible off-nominal one (dashed) for a 360° approach. The actual and nominal values of the state variables, and the deviations, are indicated for a given altitude. Notice that the guidance scheme does not attempt to restore the vehicle to the nominal path, but instead it smoothly funnels the vehicle from its off-nominal condition down to the desired terminal conditions.

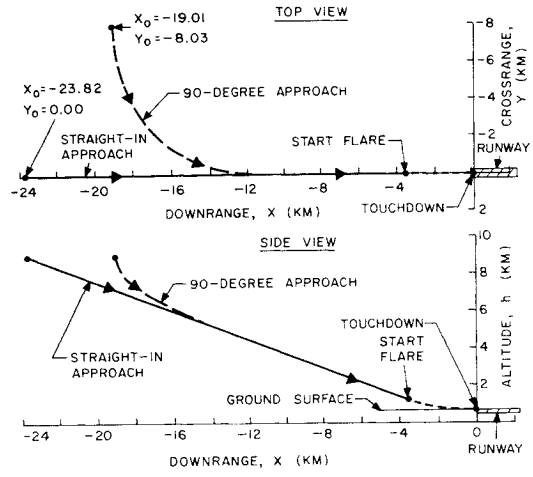

Fig. 6 Nominal trajectory profiles.

System Performance

The performance of the approach guidance scheme developed above was evaluated by means of a digital computer simulation which used the complete six-state-variable model of the vehicle [Eqs. (1–6)]. Details of the simulation program may be found in Ref. 8. The aerodynamic and physical vehicle data which were used are given in Table 1. These are representative of the NASA M-2 lifting body configuration.

Nominal Trajectories

Figure 6 depicts the two nominal trajectories selected for the numerical evaluation of the guidance scheme: 1) a straight-in approach, and 2) a 90° approach. Both nominals consist of a glide at a constant flight path angle of 21° from an altitude of 9.0 km to a final (start-flare) altitude of 1.2 km. The nominal control variable histories are given as functions of altitude in Fig. 7. The nominal initial velocity (240 m/sec) corresponds to a Mach number of 0.8 at the initial altitude. The initial downrange and crossrange coordinates are such that the flare maneuver begins at a point 500 m above the runway axis and 3.5 km short of touchdown. The runway altitude is assumed to be 700 m above sea level.

Feedback Gains

The feedback gains were calculated for each approach by integrating the matrix Riccati equation [Eq. (33)] backwards along the trajectory. Table 1 gives the values of the weighting functions used to specify the matrices $\mathbf{S}_f$ and $\mathbf{B}$ in Eq. (30). The variation of the characteristic length l with altitude is shown in Fig. 8.

The resulting feedback gains are presented in Figs. 9 and 10. Their magnitudes are small at the initial altitude (9000

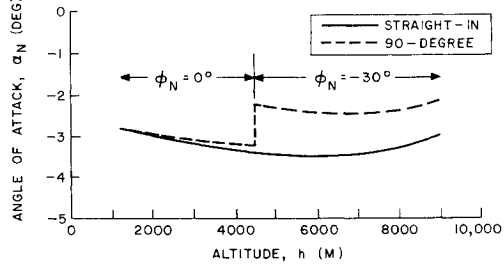

Fig. 7 Nominal α_N and ϕ_N (bank angle) control histories.

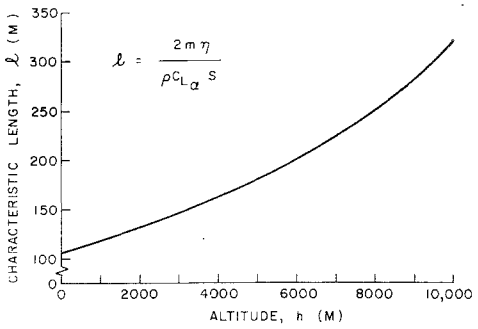

Fig. 8 Characteristic length vs altitude.

m) and grow larger as the glider descends. For the 90° approach, a discontinuity occurs in each of the gains at the roll-out altitude (4470 m) where the nominal bank angle switches from −30° to 0°. Since the two approaches are nearly identical below this altitude, the gains are practically the same.

Note that the gains $C_{\alpha y}$, $C_{\alpha\psi}$ and $C_{\phi x}$ are all zero during a straight-in glide, i.e., the longitudinal and lateral-directional controls are uncoupled. Errors in crossrange position or heading angle do not produce angle-of-attack commands, and downrange position errors do not produce bank angle commands.

In the simulation, the values of the gains and the nominal state and control histories were stored at a few selected altitudes and linear interpolation was used to calculate the the appropriate values within each altitude interval. The altitude intervals used varied from 500 m at the higher altitudes where the gains change very slowly, to 100 m near the final altitude where the gains vary rapidly.

Initial Condition Errors

Figure 11 illustrates the guidance system's performance for straight-in approaches with very large initial position and heading errors. At the top of Fig. 11 is a side view showing the nominal trajectory and those resulting from initial downrange errors of ±3000 m. It is apparent that the guidance scheme very nicely funnels the glider from its off-nominal initial position right into the nominal start-flare point. The ground tracks arising from initial heading errors of ±50° and initial crossrange errors of ±5000 m are compared with the nominal in the lower half of Fig. 11. Here again the guidance scheme performs very satisfactorily.

The effects of identical initial condition errors for the 90° approach are illustrated in Fig. 12. It is apparent that the guidance scheme is very effective for the maneuvering approach as well.

Since the terminal errors are too small to be visible on Figs. 11 and 12, Table 2 is included to clearly indicate the precise terminal accuracy of the guidance scheme. This

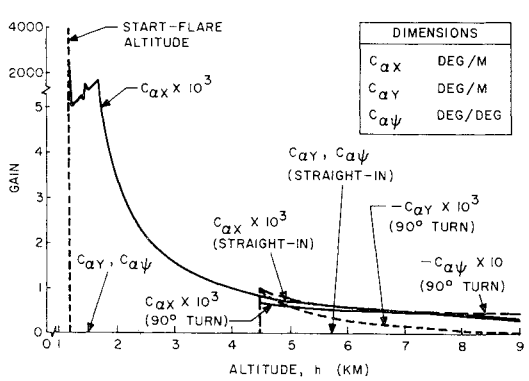

Fig. 9 Angle-of-attack feedback gains vs altitude.

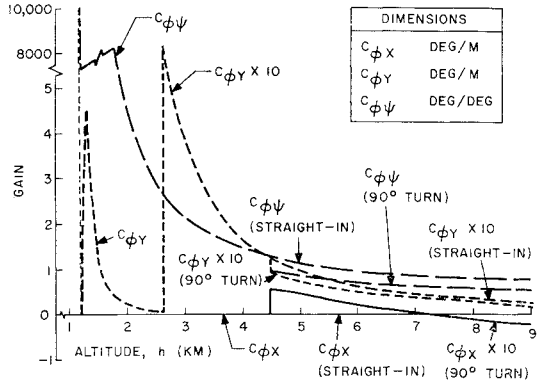

Fig. 10 Bank angle feedback gains vs altitude.

table presents the terminal errors resulting from the initial errors discussed earlier, and also those arising from initial flight path angle and velocity errors of ±6° and ±30 m/sec, respectively.

It is quite evident from these results that the proposed guidance system reduces sizeable errors at the initial altitude to very reasonable values which are well within the capability of the pilot to correct during the flare maneuver. In fact, it successfully handles errors that are well outside the valid range of the linear perturbation approximation which was used to develop the scheme.

Wind Effects

The guidance scheme and nominal trajectories were developed assuming no winds were present. However, winds will generally be encountered and it is therefore of interest to determine their effect on the guidance system's performance.

The nine different wind profiles simulated are shown in Fig. 13. Four of these are constant winds [① − ④], four are constant shears—linear variation of wind velocity with altitude [⑤ − ⑧], and one is a profile measured at the NASA Flight Research Center [⑨].** The terminal errors resulting from each of these profiles are also given in Table 2. Once again the performance of the guidance scheme is excellent. In all these cases, the disturbed trajectories were barely distinguishable from the nominals. In Fig. 14, for example, the ground tracks of the straight-in approach are shown (with a

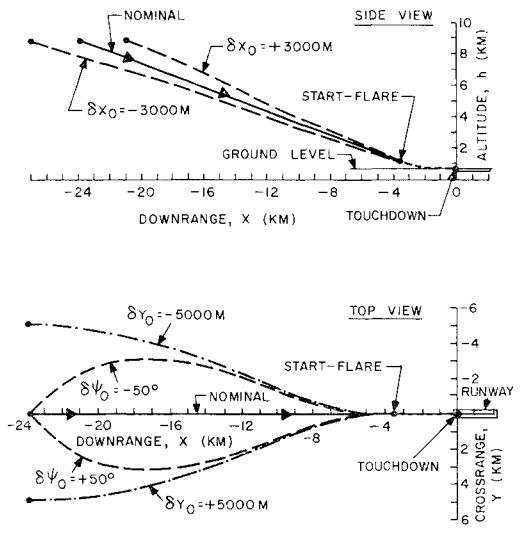

Fig. 11 Straight-in approach with initial condition errors (δx_0 at top, δy_0 and $\delta\psi_0$ at bottom).

** Measured on September 2, 1966, for flight M5-12 of the M2-F2 vehicle.

Table 2 Terminal deviations for a) off-nominal initial conditions, b) various wind profiles, and c) variations in parameters

	Straight-in approach					90° approach				
	δx_f, m	δy_f, m	$\delta\psi_f$, deg	$\delta\gamma_f$, deg	δV_f, m/sec	δx_f, m	δy_f, m	$\delta\psi_f$, deg	$\delta\gamma_f$, deg	δV_f, m/sec
a) Initial Condition Errors										
δx_0 = +3000 m	5.52	0	0	4.60	15.03	12.11	0.22	−0.17	4.45	14.12
δx_0 = −3000 m	−16.47	0	0	−3.04	−14.14	−26.41	0.01	0	−2.68	−13.49
δy_0 = +5000 m	−14.03	−0.03	−0.03	−2.47	−8.21	−17.82	0.10	−0.05	−3.34	−5.22
δy_0 = −5000 m	−14.03	0.03	0.03	−2.47	−8.21	−27.14	−0.03	0.02	−3.20	−13.40
$\delta\psi_0$ = +50 deg	−22.18	0	−0.01	−2.53	−15.94	−55.37	0.03	0	−5.38	−26.37
$\delta\psi_0$ = −50 deg	−22.18	0	0.01	−2.53	−15.94	−115.78	−2.67	0.33	2.04	8.21
$\delta\gamma_0$ = +6 deg	13.09	0	0	0.63	−2.82	15.51	0.09	0.01	0.82	−1.53
$\delta\gamma_0$ = −6 deg	−22.97	0	0	−0.08	2.93	−19.10	0.02	−0.02	0.78	1.17
δV_0 = +30 m/sec	1.94	0	0	1.93	4.21	−6.78	−0.06	−0.01	1.19	3.04
δV_0 = −30 m/sec	21.55	0	0	−0.62	−8.10	23.43	0.07	0	−0.31	−6.41
b) Wind Profiles (Fig. 13)										
① W_x = +5 m/sec	17.13	0	0	1.08	8.66	14.34	−0.12	−0.01	1.25	9.16
② W_x = −5 m/sec	−16.86	0	0	−1.28	−9.14	−13.38	0	0.01	−1.18	−9.59
③ W_y = +5 m/sec	−0.22	0.04	0	−0.02	−0.16	4.67	0.04	0	−0.15	−0.98
④ W_y = −5 m/sec	−0.22	−0.04	0	−0.02	−0.16	−2.15	−0.03	0.01	0.13	0.57
⑤ dW_x/dh = +1.5 m/sec-km	2.80	0	0	0.18	0.88	1.53	−0.01	0	0.19	0.98
⑥ dW_x/dh = −1.5 m/sec-km	−2.89	0	0	−0.18	−0.88	−1.68	0.01	0	−0.19	−0.99
⑦ dW_y/dh = +1.5 m/sec-km	0	0	0	0	−0.01	1.44	0	0	−0.01	−0.14
⑧ dW_y/dh = −1.5 m/sec-km	0	0	0	0	−0.01	−1.53	0	0	0.01	0.13
⑨ W_x and W_y measured[a]	−4.01	0.03	0	−2.10	−7.38	−19.52	0.03	0	−1.92	−8.94
c) Parameter Variations										
δm = +10%	9.45	0	0	−0.52	7.39	16.63	−0.16	0	−0.59	6.02
δm = −10%	−14.11	0	0	−0.45	−8.17	−18.25	−0.07	0.02	−0.05	−7.05
δC_L = +10%	39.59	0	0	5.64	10.46	34.89	−0.04	0.10	5.78	10.93
δC_L = −10%	−35.11	0	0	−4.23	−14.21	−44.94	0	0	−3.79	−15.27
δC_D = +10%	−43.26	0	0	−4.04	−20.06	−47.17	0.01	0	−3.68	−19.48
δC_D = −10%	58.93	0	0	5.64	19.60	53.94	−0.18	0.03	5.44	19.17
$\delta\rho$ = +10%	−13.05	0	0	−0.36	−7.38	−16.80	−0.05	0.02	−0.14	−6.36
$\delta\rho$ = −10%	9.69	0	0	−0.62	8.19	17.95	−0.18	0	−0.68	6.63

[a] Measured on September 2, 1966, for flight M5-12 of the M2-F2 vehicle.

much-expanded crossrange scale) for profiles ③, ⑦, and ⑨. It is interesting that, in general, the constant shear profiles produced smaller over-all errors than the constant winds, even though the magnitudes of the shears were considerably greater during most of the flight.

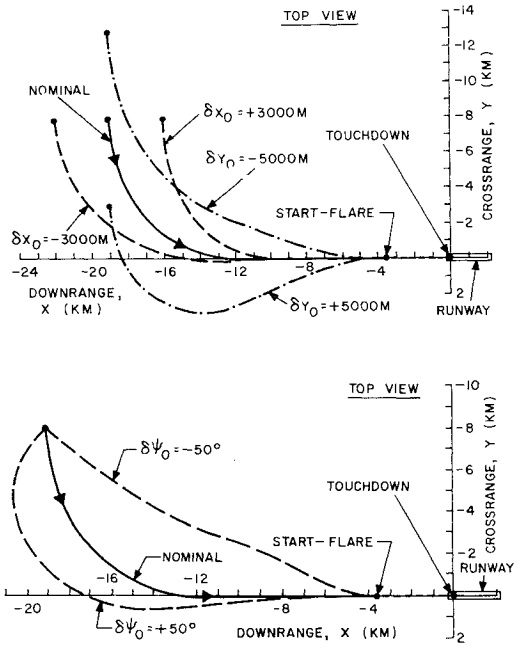

Fig. 12 90° approach with initial condition errors (δx_0 and δy_0 at top, $\delta\psi_0$ at bottom).

Other Off-Nominal Parameters

Other sources of errors are the uncertainty in the atmospheric density and in the characteristics of the vehicle itself, primarily the mass and the aerodynamic lift and drag coefficients. The atmospheric density will always differ from the model used in obtaining the feedback gains, while the vehicle characteristics—which are often not established very accurately prior to flight—may undergo significant changes as a result of mass expulsion, internal mass shifts or ablation during the initial phase of entry.

Using Ref. 9 as a guide, density variations of ±10% were selected as representing the maximum errors which might be

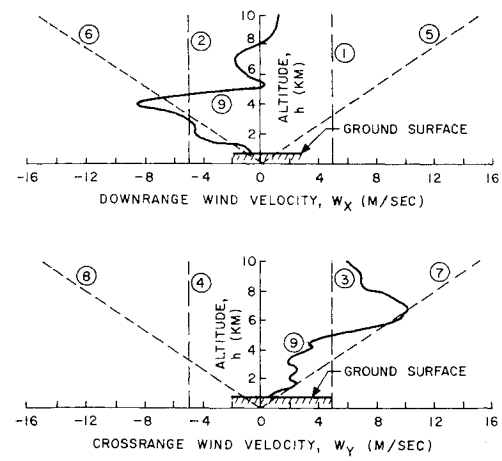

Fig. 13 Simulated wind profiles.

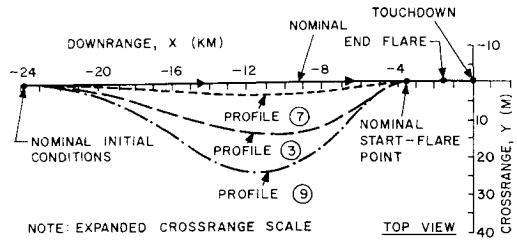

Fig. 14 Straight-in approach with wind profiles ③, ⑦, and ⑨.

encountered. Since no quantitative information was available to estimate uncertainties in the vehicle characteristics, it was assumed that these could also be determined to within 10% of their true values. Consequently, simulations were run with each of these parameters at ±10% of their nominal values. The resulting terminal errors are summarized in Table 2, which indicates that the guidance system's performance is very good in all cases. The perturbed trajectories were again very close to their nominals. For illustration, Fig. 15 presents the results of drag coefficient variations, which generally produced the largest errors.

Since the aerodynamic forces are directly proportional to the product of the atmospheric density and the reference

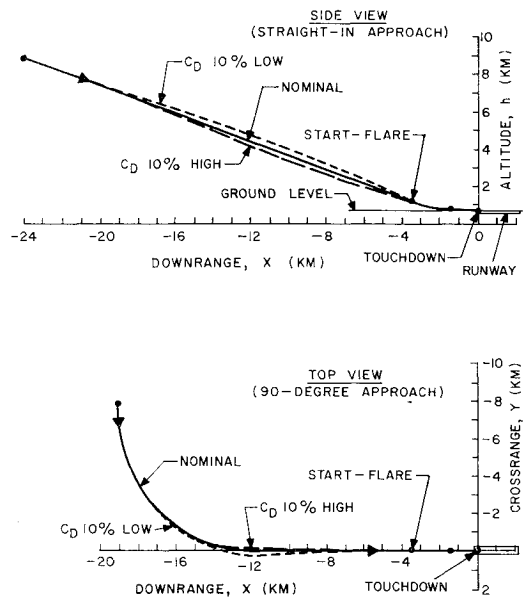

Fig. 15 Straight-in (at top) and 90° (at bottom) approaches with drag coefficient variations.

area, a given uncertainty in either S or ρ has the same effect on the performance. It is interesting that a 10% change in density, which produces a 10% change in both lift and drag, has less effect on the terminal accuracy than a 10% change in either the lift or the drag individually. Thus, the scheme is more sensitive to uncertainties in the ratio of lift to drag (L/D) than it is to errors in the total aerodynamic force.

Conclusions

The simple perturbation feedback scheme described here is capable of providing precise landing approach guidance for a lifting body entry vehicle. The guidance scheme can accommodate very large initial condition errors, winds, and variations in atmospheric density or vehicle characteristics. The complexity of the guidance law is reduced considerably by assuming a quasisteady subsonic glide and by using altitude as the independent variable. The scheme is easily implemented with modest computational and storage requirements, so that a number of nominal approaches could readily be carried onboard. This combination of large error accommodation capability and simplicity make the scheme attractive for future applications.

References

[1] Wingrove, R. C., "Survey of Atmosphere Re-entry Guidance and Control Methods," *AIAA Journal*, Vol. 1, No. 9, Sept. 1963, pp. 2019–2029.

[2] Perlmutter, L. D. and Carter, J. P., "Reference Trajectory Re-entry Guidance Without Prelaunch Data Storage," *Journal of Spacecraft and Rockets*, Vol. 2, No. 6, Nov.–Dec. 1965, pp. 967–970.

[3] Stalony-Dobrzanski, J., "Re-Entry Guidance and Control Using Temperature Rate Flight Control System," *Journal of Spacecraft and Rockets*, Vol. 3, No. 10, Oct. 1966, pp. 1441–1449.

[4] Schultz, R. L. and Anderson, P., "A Simple Guidance Scheme for Lifting Body Re-entry Vehicles," AIAA Paper 67-136, New York, 1967.

[5] Speyer, J. L. and Bryson, A. E., "A Neighboring Optimum Feedback Guidance Scheme Based on Estimated Time-To-Go With Application to Re-entry Flight Paths," *AIAA Journal*, Vol. 6, No. 5, May 1968, pp. 769–776.

[6] Hoffman, W. C., Bryson, A. E., Jr., and Zvara, J., "A Terminal Guidance Scheme for Lifting Body Entry Vehicles," NASA CR-86126, Oct. 1968, Kaman AviDyne, Burlington, Mass.

[7] Bryson, A. E. and Ho, Y. C., *Applied Optimal Control*, Blaisdell, Waltham, Mass., 1969.

[8] McKeon, K. A. et al, "Six-Degree of Freedom Analysis of Lifting Entry Vehicle Terminal Landing; Vol. II, Computer Program LIFT User's Manual," TR-45, June 1967, Kaman AviDyne, Burlington, Mass.

[9] *U.S. Standard Atmosphere Supplements, 1966*, U.S. Government Printing Office, Washington, D.C., 1966.